# Altitude profile of ion production and ionization effect at the Regener-Pfotzer region during the GLE 71 on 17 May 2012

Alexander Mishev[1,2], Peter I.Y. Velinov[3]
[1] Sodankylä Geophysical Observatory, University of Oulu, FI-90570 Oulu, Finland
[2] Space Physics and Astronomy Research Unit, University of Oulu, FI-90570 Oulu, Finland
[3] Institute for Space Research and Technology, Bulgarian Academy of Sciences, BG-1113, Sofia, Bulgaria
alexander.mihev@oulu.fi
(Submitted on 02.06.2023; Accepted on 28.08.2023)

**Abstract.** Precipitating high-energy particles from outer space, specifically with galactic origin viz. cosmic rays, consisting mostly of protons, alpha particles and heavier nuclei when penetrating the Earth's atmosphere induce a complicated nuclear-electromagnetic-meson cascade of secondary particles. A great amount of the primary particle energy is dissipated in the atmosphere by ionization of the ambient air. Occasionally, the Sun accelerates particles to the high-energy range, which similarly to the galactic cosmic rays (GCRs) induce a shower of secondary particles. The induced by cosmic rays atmospheric ionization may influence atmospheric chemistry and physics. Because the flux of the solar protons is usually significantly greater than that of the galactic cosmic rays, these effects can be enhanced during solar proton events. Hence, energetic solar particles could produce a significant excess of ion pair production, specifically over the polar caps. Herein, using Monte Carlo simulations and derived from ground-based data, cross-calibrated by direct space-borne measurements solar proton spectra, we computed the ion production rate and the corresponding ionization effect in the Earth atmosphere during the ground level enhancement (GLE) 71 occurred on 17 May 2012.
**Key words:** cosmic rays, ground level enhancement (GLE), atmospheric ionization, Monte Carlo, atmospheric physics and chemistry

## 1 Introduction

The current paradigm of the origin of cosmic rays (CRs), representing an omnipresent flux of subatomic high-energy particles, consisting mostly of protons and alpha-particles and small amounts of heavier nuclei, is that they are produced during and following supernova explosions in the galaxy, yet the most energetic ones are with extragalactic origin [Gaisser et al., (2016)]. The energy of a typical CR particle spans from about $10^7$ eV/n, energy per nucleon, up to extreme energies of about $10^{21}$ eV/n. CRs constantly penetrate the Earth's atmosphere and by successive interactions induce a complicated nuclear-electromagnetic-meson cascade of secondaries, that is, extensive air shower (EAS) (Auger cascade) [Grieder, (2011), Gaisser et al., (2016)]. A great amount of the primary particle energy is dissipated in the atmosphere, eventually leading to ionization of the ambient air [Mironova et al., (2015)].

For instance, a CR proton and/or heavier nucleus when entering the atmosphere produce energetic secondary particles, mostly hadrons, pions and kaons. The bulk of those secondary particles decay almost instantly to another, next generation of particles, that is, the short-living particles decay, produce other particles and/or emit Bremsstrahlung. Neutral pions decay mostly into two gammas, the latter producing electron-positron pairs, yet decays into electron-positron pairs (Dalitz decay) are also possible. Hence, such sub-cascade within the Bremsstrahlung radiation, determines the evolution of the electromagnetic

component of the EAS. Charged pions mostly decay into muons, giving rise of the muon component of the EAS. The cascade develops until threshold energy for the production of new particles is reached. We would like to emphasize that at each hadron interaction, about one-third of the energy is transferred to the electromagnetic component of the shower [Grieder, (2011),Gaisser et al., (2016)], and because the majority of the secondary hadrons re-interact, and due to the rapid multiplication of electromagnetic cascades, the electrons and the positrons are the most numerous charged particles in the Auger cascade. Therefore, an essential part of the primary CR energy is dissipated by ionization losses of the electrons and positrons. The maximum ion production is observed at an altitude of about 12–15 km above sea level, known as Regener–Pfotzer maximum [Regener and Pfotzer (1935)].

The flux of galactic cosmic rays (GCRs) is modulated in the Heliosphere, so that it inversely follows the 11-year solar cycle [Potgieter, (2013)]. While the GCRs determine the background ionization in the atmosphere, specifically in the stratosphere, active processes on the Sun leading to acceleration of high-energy particles, that is solar energetic particles (SEPs) [Reames, (1999)], can significantly enhance the atmospheric ionization, see for details [Usoskin et al., (2011), Velinov et al., (2013), Mishev and Velinov, (2015), Mishev and Velinov, (2018)], yet transients (e.g. Forbush decreases of the CR flux) can partially compensate the ionization [Mishev and Velinov, (2020), Dorman et al., (2022)]. Precipitating energetic particles impact ionization is very important for revealing and quantification of their influence on different atmospheric processes, global electric circuit, and atmospheric physics and chemistry, specifically the minor components [Mironova et al., (2015)]. Here we focus on a specific class of strong SEPs, which can be registered at the ground level by convenient detectors, e.g. neutron monitors (NMs), called ground-level enhancements (GLEs) [Shea and Smart, (1982),Poluianov et al., (2017)]. In this case, accelerated solar ions may cause a significant excess in atmospheric ionization, specifically over the polar caps [Usoskin et al., (2011)]. Here, we study a specific GLE event of the previous Solar Cycle 24, that is, GLE 71, which occurred on 17 May 2012.

## 2 The GLE 71 on 17 May 2012: spectra and features

The event on 17 May 2012, that is GLE 71 resulted from eruptive processes in the active region NOAA 11476, namely a class M5.1 solar flare with onset observed at 01:25 UT and a coronal mass ejection (CME) firstly observed by the C3 coronograph on SOHO satellite at 02:06 UT, with an estimated speed of about 1200 km $s^{-1}$. Detailed information is presented in several web based sources e.g.

*https://www.ngdc.noaa.gov/stp/satellite/goes/dataaccess.html*,

*https://izw1.caltech.edu/ACE/ASC/level2/lvl2DATA_EPAM.html*, OMNI web service:

*https://omniweb.gsfc.nasa.gov/*, as well as catalogs e.g. [Miteva et al., (2013), Papaioannou et al., (2016)].

We note that the active region was on the west side of the Sun, namely at N07 W88, so that the Earth could be regarded to be relatively well magnetically connected to the eruption core. The global NM network recorded the

event as a weak enhancement of the count rates of several stations, specifically those located in the polar region. We emphasize that only Apatity, Oulu and the South Pole NMs revealed weak count rate increases, yet below 20 %, whilst the majority of the NMs exhibited marginal count rate increases Fig. 1. Therefore, a large anisotropy of the arriving SEPs in the vicinity of the earth was implied, confirmed by several studies [Bruno et al., (2018),Kocharov et al., (2018)]. Most notably, a peculiar angular distribution was revealed, that is, particles arriving from the Sun following the Parker spiral, as well as a shifted significant amount of solar protons arriving from the anti-Sun direction, the latter due to complicated interplanetary transport, namely lost cone scenario [Mishev et al., (2014)], a feature discussed in great details elsewhere [Ruffolo et al., (2006)].

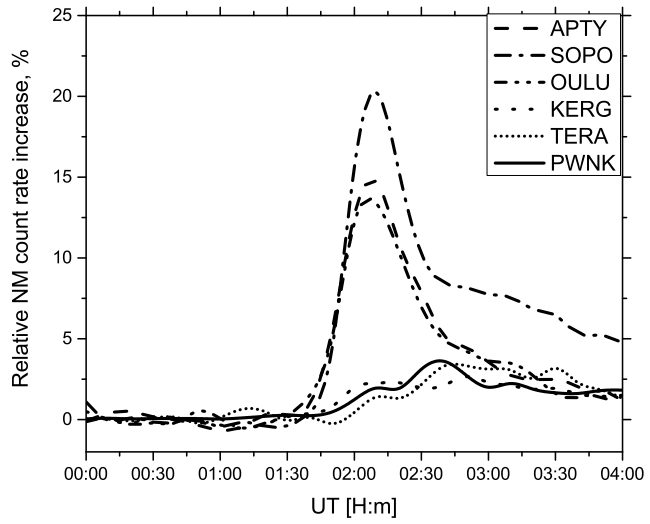


**Fig. 1.** Spline smoothed NM count rates of selected stations as denoted in the legend during GLE 71.

In order to compute the ion production rate in the atmosphere it is necessary to possess reliable information about the SEP spectra [Mishev (2023)]. During the GLE 71 the rigidity spectra of the SEPs revealed a modified power-law spectral shape as considered by [Cramp et al., (1997), Vashenyuk et al., (2006)]:

$$J_{||}(P) = J_0 P^{-(\gamma+\delta\gamma(P-1))} \tag{1}$$

where $J_{||}(P)$ is the particle flux with given rigidity $P$ in [GV] arriving from the Sun along the axis of symmetry, which is defined by the geographic coordinate

angles $\Psi$ and $\Lambda$ (latitude and longitude). In Eq. 1, $\gamma$ is the power-law spectral exponent at rigidity P = 1 GV, accordingly $\delta\gamma$ is the rate of the spectrum steepening. Accordingly, the angular distribution of the arriving SEPs was depicted by a complicated pitch angle distribution (PAD) with shape similar to that considered by [Cramp et al., (1997), Mishev et al., (2014)], namely superposition of two Gaussians:

$$G(\alpha(P)) \sim \exp(-\alpha^2/\sigma_1^2) + B \cdot \exp(-(\alpha - \alpha^{'})^2/\sigma_2^2) \tag{2}$$

where $\alpha$ is the pitch angle, $\sigma_1$ and $\sigma_2$ are parameters corresponding to the width of the pitch angle distribution, $B$ and $\alpha^{'}$ are parameters corresponding to the contribution of the second Gaussian, including direction nearly opposite to the derived axis of symmetry, precisely $B$ corresponding to the amount of anti-Sun particle flux.

An illustration of the of the event averaged spectrum and PAD is presented in Fig. 2, while the details are given in [Mishev et al., (2021), Pätsi and Mishev (2022)]. Here the characteristics of the mean spectrum and PAD are as follows: $J_0$=1.21×10$^5$ [m$^{-2}$ sr$^{-1}$, s$^{-1}$ GV$^{-1}$], $\gamma$ = 7.63, $\delta\gamma$=0.07, $\sigma_1^2$=2.5 [rad$^{-2}$], $\sigma_2^2$=2.35 [rad$^{-2}$] and $B$=0.58. One can see that despite the complicated angular distribution of the SEPs in the vicinity of the earth, a nearly isotropic distribution averaged over the whole event is revealed, presented on the right-hand panel of Fig. 2.

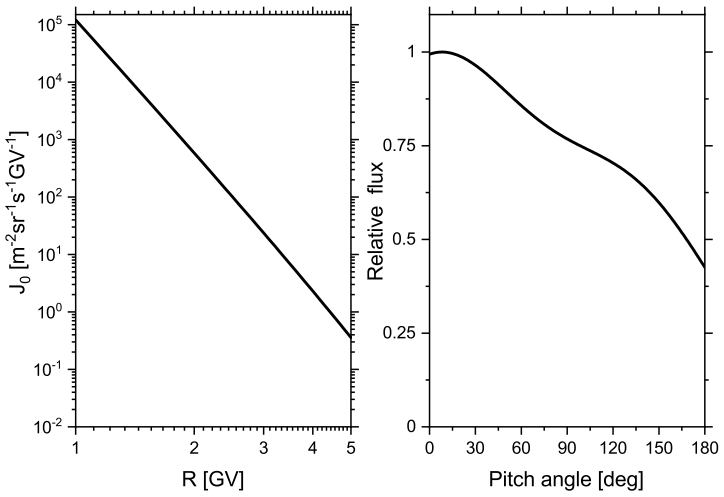


**Fig. 2.** Event averaged spectrum and angular distribution during GLE 71.

## 3 Employed model for computation of the energetic particles impact ionization

Basically, the ion production rate in the atmosphere due to CRs of galactic and/or solar origin can be computed using analytical(empirical models), however they generally possess constraints since they are usually limited to a given atmospheric region e.g. upper atmosphere, or primary particle species [Velinov et al., (2013), Mironova et al., (2015)].

Nowadays, the development of more sophisticated models, based on Monte Carlo simulations e.g. [Desorgher et al.(2005), Usoskin and Kovaltsov (2006), Velinov et al.(2009)], that is full target models, allows one to consider realistically and in great detail the propagation of high-energy particles in the atmosphere of the Earth, namely to follow the evolution of the induced by CRs cascade and to obtain with reasonable precision the deposited energy by the different EAS components.

In this study, we employed a Monte Carlo-based model, which follows the work by [Usoskin and Kovaltsov (2006)], the full description and applications to which are presented elsewhere [Velinov et al.(2009), Mishev and Velinov, (2020), Dorman et al., (2022)].

The ion production rate in ion pairs/s.cm$^3$ at a given altitude altitude $h$ above sea level is given by:

$$q(h,E) = \frac{1}{E}_{ion} \sum_i \int_{E(P_c)}^{\infty} \int_{\Omega} J_i(E) Y(h,E) \rho(h) dE d\Omega \tag{3}$$

$h$ is the air overburden (air mass) above a given altitude in the atmosphere expressed in g/cm$^2$ or altitude, $J_i(E)$ is the differential cosmic ray spectrum for a given component $i$: protons p, Helium ($\alpha$-particles) the latter effectively accounting for heavier nuclei [Mishev and Velinov (2011)], $\rho$ is the atmospheric density in g/cm$^3$, $E$ is the energy of the incoming primary CR nuclei, $\Omega$ is a solid angle and $E_{ion} = 35$ eV is the average energy necessary to yield an ion pair in air [Porter et al., (1976)]. The integration is over the kinetic energy $E(P_c)$ above the rigidity cut-off $P_c$ for a nuclei of type $i$ at a given geographic location by the expression:

$$E_{cut,i} = \sqrt{\left(\frac{Z_i}{A_i}\right)^2 P_c^2 + E_0^2} - E_0 \tag{4}$$

where $E_0 = 0.938$ GeV/n is the proton's rest mass and the ionization yield function and given altitude $h$ or mass overburden is defined as:

$$Y(h,E) = \frac{\partial E(h,E)}{\partial h} \tag{5}$$

where $\partial E$ is the deposited energy in an atmospheric layer $\partial h$. The yield function, that is the response matrix, represents the response of the ambient air at a given atmospheric depth as deposited energy (ionization) to a mono-energetic unit flux of primary particle entering the Earth's atmosphere. In Eq.3 the mass overburden, that is, the atmospheric depth is expressed in g/cm$^2$, which can

be eventually converted to altitude. We emphasize that the mass overburden is naturally related to the particle shower development.

Eq. 3 allows one to compute the ion production rate due to SEPs and GCRs. Here, for the former we employed the derived spectra during GLE 71, whilst for the latter we employed the force field model [Caballero-Lopez and Moraal (2004)], where the parameterization of the local interstellar spectrum is according to [Vos (2015)]. All computations are performed using a realistic atmospheric model NRLMSISE-00 [Picone et al., (2002)].

## 4 Ion production rate and ionization effect during GLE 71

Employing the aforedescribed model, namely Eqs. 3–5, and using the derived SEP spectra during GLE 71, we computed the full altitude profile of ion production rate in the atmosphere at several rigidity cut-offs, presented in Fig. 3 during the considered in this study GLE. The computations were performed at regions with marginal geomagnetic shielding, that is, polar and sub-polar ($P_c$ =0 GV and $P_c$ =1 GV rigidity cut-off, respectively), presented in Fig. 3a and Fig. 3b, and high mid-latitude regions with $P_c$ = 2 GV (Fig. 3c). We emphasize that the axes of Fig. 3 are inverted in order to present the ion production rate naturally as a function of the altitude, that is the altitude is given in Y-axis, whilst the ion rate in X-axis. Such a type of presentation allows straightforward interpretation of the computations and to clearly see the shift of the Regener-Pfotzer maximum as a function of the rigidity cut-off. We note that the ion production rates at various stages of the event is presented as a superposition of GCRs and SEPs contributions, whilst the contribution of solely GCRs is given separately.

One can see that the ion production rate due to SEPs was greater than that due to the GCRs, yet at regions with $P_c \geq 2$ GV dominates the contribution of the latter. Besides, the ion production rate during the event onset (02:00UT), when the SEP spectra were harder than during the late phase of the event (03:00UT), was significantly greater. In addition, the maximum of ion production due to the solar protons was higher in the atmosphere compared to the Regener-Pfotzer maximum due to the GCRs, because of the softer spectra of the former. For example the maximum of ion production rate during GLE 71 over the polar cusp was about 350 ion pairs/s at an altitude of about 30 km above sea level, whilst the ion production rate due to GCR in quiet solar conditions was about 60 ion pairs/s at an altitude of 12 km. While at high-mid latitudes with $P_c < 2$ GV, the ion production due to SEPs was comparable to the average contribution of GCRs, over the polar cusp, the contribution of SEPs is notably greater, yet at mid-latitudes, the contribution of GCRs dominated, as it is clearly seen in the position in the maximum in Fig. 3c).

Next, we computed the net ionization effects, normalized to 24h, over the GLE 71, in the vicinity of the Regener-Pfotzer maximum [Regener and Pfotzer (1935)], that is, at depths of 150 and 250 g/cm$^2$, respectively, shown in Figs. 4-5 For this purpose, we computed the rigidity cut-offs over the globe in a grid of 1°x1°, employing a realistic magnetospheric model, namely a combination of the IGRF geomagnetic model as the internal field and the Tsyganenko 89 model [Tsyganenko, (1989)] as the external field. Subsequently, considering explicitly the evolution of the SEP spectra throughout the event, namely

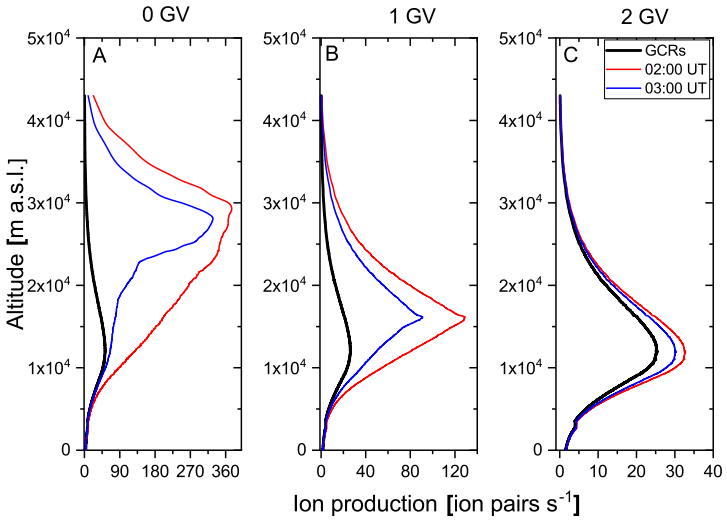


**Fig. 3.** Ion production rate as a function of the altitude during the initial (02:00 UT) and late phase (03:00 UT) of GLE 71 due to GCRs and SEPs as denoted in the legend.

their softening, we computed the ion production and the relative to the GCRs ionization effect. One can see that the net ionization effect during GLE 71 maximizes over the polar caps (about 20 % at depth of 150 g/cm$^2$ and 15 % at depth of 250 g/cm$^2$, respectively), whilst in the mid and low latitude regions it is considerably smaller, even marginal in the equator, due to the softer SEP spectra in comparison to the GCRs.

## 5 Conclusion

Here, employing derived on the basis of ground-based NM measurements SEP spectra and state-of-the-art 3-D full target model, we computed as realistically as possible, the ion production and the corresponding ionization effect in the Earth's atmosphere, specifically in the region of Regener-Pfotzer maximum, during a specific strong solar proton event, that is, GLE 71 on 17 May 2012. In this study we provided the altitude profile of the ion production, separately for the GCR, as well as a superposition of SEPs and GCRs contributions, at several rigidity cut-offs (0-1GV and 2 GV), corresponding to polar and sub-polar for the former, and high mid-latitude region for the latter. In addition, we provided global maps with a resolution of 1°x1° of the ionization effect in the region corresponding to the Regener-Pfotzer maximum, which over the polar caps was about 20 % at depth of 150 g/cm$^2$ and 15 % at depth of 250 g/cm$^2$, respectively. The results presented here allow one to quantify the impact of high-energy precipitating particles on atmospheric chemistry and physics and give a good basis for further studies related to space weather.

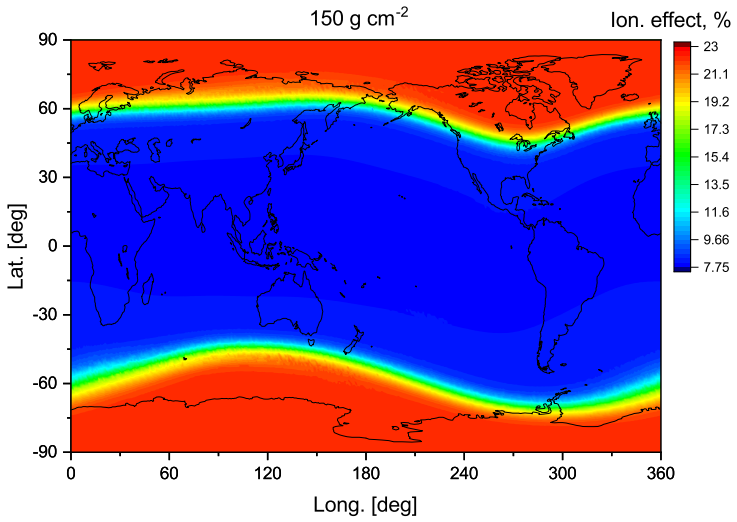


**Fig. 4.** Global map of 24h averaged ionization effect in the atmosphere at depth of 150 g/cm$^2$ during GLE 71.

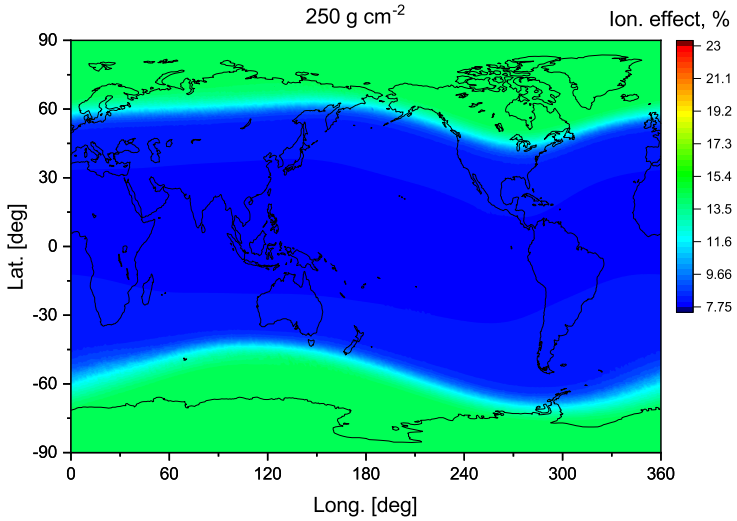


**Fig. 5.** Global map of 24h averaged ionization effect in the atmosphere at depth of 250 g/cm$^2$ during GLE 71.

Precise and detailed study of the induced ionization due to precipitating high-energy particles, specifically GLE-causing SEPs, is important in order to

quantify the influence of energetic particles on different processes related to the physics and chemistry of the minor components in the Earth's atmosphere. We would like to emphasize, that such processes can be studied during GLEs in enhanced mode, because of the considerably increased particle flux in the atmosphere during GLE events as such. As it was shown [Mironova et al., (2015)], the energetic particles impact ionization is particularly interesting to investigate during GLEs, namely under specific conditions e.g. reduced solar UV. Therefore, for realistic quantification of the influence of precipitating high-energy particles on atmospheric minor constituents, it is necessary to compute the ionization effect at various time scales, preferably on a global scale, as well as to provide an altitude profile. Therefore, the presented here, peculiar in terms of angular distribution, GLE 71, namely the induced by SEPs atmospheric ionization in the region of Regener-Pfotzer maximum, is important to deepen the knowledge in the field, as well as to verify the existing models and other tools.

## Acknowledgements

This work is dedicated to the memory of L.I. Dorman passed away in July 2022, a colleague and friend, with a very bright long scientific carrier, lasting from the first detection of the strongest ever registered GLE in 1956 till the last months. Part of this work was supported by the Academy of Finland (project 330063 QUASARE and 321882 ESPERA ). The work was also supported by HE program, project ALBATROS. This work was partially supported by the National Science Fund of Bulgaria under contract KP-06-H28/4.

## References

Bruno, A. et al., 2018. *Astrophysical Journal* 862, 97.
Caballero-Lopez, R. and Moraal, H., 2004. *Journal of Geophysical Research* 109, A01101.
Cramp, J. et al., 1997. *Journal of Geophysical Research* 102, A11 24,237–24,248
Desorgher, L. et al., 2005. *International Journal of Modern Physics A* 20, 6802–6804.
Dorman L. et al., 2022. *Advances in Space Research* 70, 253–260.
Gaisser, T., et al., 2016. Cosmic Rays and Particle Physics. Cambridge University Press, Cambridge, UK. ISBN 9781139192194.
Grieder, P., 2011. Extensive Air Showers: High Energy Phenomena and Astrophysical Aspects - A Tutorial, Reference Manual and Data Book. Springer, Space Science Library Book 1009. ISBN 978-3540769408.
Kocharov, L. et al., 2018. *Astrophysical Journal Letters* 862, L20.
Mironova, I. et al., 2015. *Space Science Reviews* 194, 1-96.
Mishev, A., 2023. *Journal of Atmospheric and Solar-Terrestrial Physics* 243, 106021.
Mishev, A. and Velinov, P., 2011. *Advances of Space Research* 48, 19–24.
Mishev A. and Velinov P., 2015. *Journal of Atmospheric and Solar-Terrestrial Physics* 129, 78–86.
Mishev, A. and Velinov P., 2018. *Advances in Space Research* 61, 316–325.
Mishev A. and Velinov P., 2020. *Journal of Atmospheric and Solar-Terrestrial Physics* 211, 105484.
Mishev, A. et al., 2014. *Journal of Geophysical Research* 119, 670–679.
Mishev, A. et al., 2021. *Space Weather* 19, 2, e2020SW002626.
Miteva, R. et al., 2013. *Solar Physics* 282, 2, 579-613.
Papaioannou, A. et al., 2016. *Journal of Space Weather and Space Climate* 6, A42.
Picone, J. et al., 2002. *Journal of Geophysical Research: Space Physics* 107, 1468.
Poluianov, S. et al., 2017. *Solar Physics* 292, 176.
Pätsi, S. and Mishev, A., 2022. *Advances in Space Research* 69, 2893 – 2901.

Porter, H. et al., 1976. *The Journal of Chemical Physics* 65, 154–167.
Potgieter, M., 2013. *Living Reviews in Solar Physics* 10, 3.
Reames D., 1999. *Space Science Reviews* 90 413–491.
Regener, E. and Pfotzer G., 1935. *Nature* 136, 718–719.
Ruffolo, D. et al., 2006. *Astrophys. J.* 639(2), 1186–1205.
Shea, M. and Smart D., 1982. *Space Science Reviews* 32, 251–271.
Tsyganenko, N, 1989. *Planetary and Space Science* 37, 5–20.
Usoskin, I. and Kovaltsov, G., 2006. *Journal of Geophysical Research* 111.
Usoskin I. et al., 2011, *Atmospheric Chemistry and Physics* 11, 1979–1988.
Vashenyuk, E. et al., 2006. *Advances Space Research* 38, 3, 411–417.
Velinov, P. et al., 2009. *Advances Space Research* 44, 1002–1007.
Velinov P. et al., 2013. *Journal of Space Weather and Space Climate* 3, A14.
Vos E. 2015, *Astrophysical Journal* 815, 119.